Use of Green Fluorescent Protein-Conjugated β-Actin as a Novel Molecular Marker for in Vitro Tumor Cell Chemotaxis Assay

Louis Hodgson,[†] Wei Qiu,[†] Cheng Dong,[†] and Andrew J. Henderson*[,‡]

Department of Bioengineering, 229 Hallowell Building, and Department of Veterinary Science, 115 Henning Building, Pennsylvania State University, University Park, Pennsylvania 16802

To study the dynamics of actin cytoskeleton rearrangement in living cells, an eukaryotic expression vector expressing a β-actin−GFP fusion protein was generated. The expression construct when transfected into NIH3T3 fibroblast, A2058 human melanoma and 293T human embryonic kidney carcinoma cell lines expressed β-actin−GFP fusion protein, which colocalized with endogenous cellular actin as determined by histoimmunofluorescence staining. The β-actin−GFP was also observed to be reorganized in response to treatments with the chemoattractant type IV collagen. Cells extended pseudopodial protrusions and altered the morphology of their cortical structure in response to type IV collagen stimulation. More importantly, β-actin−GFP accumulated in areas undergoing these dynamic cytoskeleton changes, indicating that β-actin−GFP could participate in actin polymerization. Although ectopic expression of β-actin−GFP lead to minor side effects on cell proliferation, these studies suggest that this strategy provides an alternative to the invasive techniques currently used to study actin dynamics and permits real-time visualization of actin rearrangements in response to environmental cues.

Introduction

In response to environmental cues such as growth factors, extracellular matrix (ECM) components, and chemokines, motile cells will undergo dramatic changes in cell morphology including continuous cycling of protrusions, reabsorption of pseudopods, and crawling *(1−4)*. The ability of cells to detect and respond to chemoattractant gradients is critical for cell migration during embryogenesis, mobilization of leukocytes to sites of inflammation, and metastasis of tumor cells. Morphological changes that permit cell motility are dependent on the dynamic properties of the actin cortical network. In addition to regulating cell migration, remodeling of actin filaments can influence cell functions including proliferation, differentiation, organization of membrane receptors, and signal transduction *(1, 5, 6)*. Therefore, understanding the organization of the cytoskeleton and, in particular, the dynamics of actin filaments is critical for elucidating the underlying mechanisms that regulate multiple cellular functions.

Most studies investigating the dynamics of actin microfilament networks and their rearrangement during cell motility have relied on fluorescently tagged actin monomers. Such experiments require either microinjecting prelabeled G-actin into individual cells or visualizing actin filaments and monomers by histoimmunofluorescence on fixed cell populations *(1, 7−10)*. Although these studies have provided insight into the association of actin monomers and their polymerization, they are extremely invasive and introduce potential artifacts, especially if collecting fluorescence data.

Green fluorescent protein (GFP) has been a useful tool in marking and labeling cells in vivo and in vitro *(11−17)*. GFP is relatively innocuous and can be detected in living cells with little preparation. Furthermore, GFP−actin fusion proteins have successfully been expressed in *Dictyostelium*, yeast, and *Drosophila*, as well as in a variety of mammalian cell lines *(18−21)*; however, the use of such approaches in functional assays involving mammalian cells has been limited. Previous studies have used GFP−actin to observe changes in the actin cytoskeleton in migrating tumor cells as well as actin reorganization in a host cell following *Listeria monocytogenes* infection *(12, 13)*. In this study, we have employed a fusion protein of β-actin with enhanced green fluorescent protein for real-time visualization of actin remodeling during chemotaxis and pseudopodial protrusion assays in mammalian cells. We report the first in vitro observations of actin dynamics in a viable tumor cell during an active chemotactic response toward type IV collagen.

Materials and Methods

***β*-Actin−GFP Fusion Expression Vector.** Human β-actin cDNA was PCR-amplified using a pair of oligonucleotide primers, 5′-gtcggatccgaagcatttgcggtggacgatgga-3′ and 5′-ttcgaattcctcaccatggatgatgatatcgccg-3′ (Gibco BRL, MD) from a β-actin−pUC18 plasmid obtained from I. M. A. G. E. Consortium. The resulting PCR product (1126bp) was agarose gel-purified and digested with Eco RI and Bam HI. The purified fragments were subcloned in-frame into Eco RI/Bam HI digested pEGFP−N3 expression vector (Clontech Inc., CA) using T4 ligase. Under CMV IE promoter, this construct (pβ-actin−GFP) expressed a full-length β-actin protein that had GFP fused to the carboxy terminus.

* Telephone: (814)-865−7696. Fax: (814)-863−6140. E-mail: ajh6@psu.edu.
[†] Department of Bioengineering.
[‡] Department of Veterinary Science.

10.1021/bp000093o CCC: $19.00
Published on Web 09/26/2000

β-Actin−GFP and pEGFP were introduced into *Escherichia coli* DH5α by $CaCl_2$ transformation following standard protocols *(22)*. Transformed cells were selected for antibiotic resistance by plating on LB agarose plates (1% bacto-tryptone, 0.5% bacto-yeast extract, 1% NaCl, 1.5% bacto-agar in 1 L of H_2O and adjusted to pH 7.0) containing 50 μg/mL kanamycin sulfate (Eastman Kodak, NY). Plasmid DNA preparations from individual bacterial colonies were purified using a Jetstar Plasmid Miniprep kit (Jetstar GmbH, Germany), and the integrity of the DNA was confirmed by restriction digest analysis.

Cell Transfection. The NIH3T3 cell line was maintained in RPMI 1640 supplemented with 10% fetal bovine serum (FBS; Biofluids Inc., MD). The A2058 human melanoma and 293T human embryonic kidney carcinoma cell lines were maintained in Dulbecco's modified Eagle's medium (DMEM) supplemented with 10% FBS (Biofluids Inc.). The NIH3T3 and A2058 cells were transfected using Lipofectamine2000 reagent (Gibco BRL, MD). Cells were cultured to reach 90−95% confluence in six-well plates containing 25 mm round glass coverslips (pretreated with 0.1% gelatin solution overnight). Aliquots (5 μg) of pβ-actin−GFP or pEGFP DNA and 10 μL of Lipofectamine2000 reagent solution were added to 250 μL each of Opti-MEM I (Gibco BRL) and were incubated at room temperature for 5 min. Two solutions were mixed and incubated for 20 min to allow DNA−liposome complex formation. This transfection solution was added to the standard culture medium. Cells were cultured in the transfection mixture for 12 h, at which time the media was replaced with fresh 10% FBS in DMEM. 293T cells were plated onto 60 mm tissue culture plates or 25 mm round glass coverslips at a concentration of 1×10^6 cells/mL in 35 mm tissue culture plates approximately 12 h prior to the calcium phosphate transfection. Aliquots (10 μg) of pβ-actin−GFP or pEGFP DNA, 0.12 M $CaCl_2$, and 2× HEPES balanced saline (1.6% NaCl, 0.074% KCl, 0.027% $NaHPO_4 \cdot 2H_2O$, and 0.2% dextrose plus 1% HEPES at pH 7.05) were mixed and added to the standard culture medium. Cells were cultured in the transfection mixture for 5 h, at which time the media was replaced with fresh 10% FBS in DMEM. Transfection efficiency was assessed by GFP expression 18−24 h post-transfection by fluorescence microscopy or flow cytometry.

Western Blot. Whole-cell extracts were prepared by resuspending 1×10^7 cells in 200 μL of 2× SDS running dye (0.2% bromophenol blue, 4% SDS, 100 mM Tris [pH 6.8], 2 mM DTT, 3 ng/mL aproptinin, 2 ng/mL pepstatin A, 1 ng/mL leupeptin, 0.8 mM PMSF, 1 mM AEBSF, 50 μM bestatin, 15 μM E−64, and 30% glycerol). Aliquots (20 μL) were loaded onto an 8% SDS−PAGE gel, and the protein was transferred to 0.2 μm nitrocellulose filter (Schleicher and Schuell, NH) by electroblotting. The filter was blocked for 1 h in phosphate buffered saline containing 0.2% Tween-20 (PBST) with 5% nonfat milk (NFM). β-Actin was detected by diluting mouse anti-β-actin IgG1 (Sigma Chemical Co., MO) 1:2500 in PBST plus 5% NFM and incubating overnight at 4 °C. Following incubation with the primary antibody, the filter was washed with PBST at 24 °C three times before the secondary antibody was added (peroxidase-conjugated goat anti-mouse IgG diluted 1:5000 in PBST with 5% NFM). After 1 h of incubation, the filter was washed in PBST three times followed by a single wash in PBS. Proteins were detected using the enhanced chemiluminescence detection system (Amersham Lifescience, CA). The filter was subsequently stripped of antibodies by incubating for 30 min at 70 °C in 62.5 mM Tris-HCl, 100 mM β-mercaptoethanol, and 2% SDS. Following incubation, the filter was washed three times in PBST and reprobed using a rabbit anti-GFP peptide IgG (Clontech, Inc.) diluted 1:100 in PBST with 5% NFM as described above except that the secondary antibody was goat anti-rabbit IgG. The protein detection protocols used in this case were similar to the initial β-actin detection.

Cell Fixation and Immunofluorescence Staining Assay. Spreading cells on a glass cover slip were fixed using 10% formaldehyde in PBS for 30 min and washed three times in PBS. Fixed cells were treated for 20 min with 0.3% Triton-X100 to permeabilize the cell membrane, followed by three successive PBS washes. Texas Red conjugated DNase I and Alexa Fluor 488 or 568 conjugated phalloidin (Molecular Probes Inc., OR) were added to the fixed and permeabilized cells at concentrations of 0.3 μM and 10 units, respectively, and incubated for 40 min in order to specifically label the cytoplasmic actin. The immunofluorescence stained plates were washed three times in PBS and observed using a fluorescence microscope at excitation/emission wavelengths of 596/620, 488/520, and 570/603 (in nanometers), respectively.

Cell Sorting and Microchemotaxis Assay. A Coulter EPICS 753 (Coulter Co., FL) flow cytometer was used to quantitate and sort cells that expressed β-actin−GFP conjugated protein. The transfected cells were detached when subconfluent by a brief trypsinization and were resuspended in culture media at a concentration of 1×10^7 cells/mL. The cell sorting was performed after obtaining the basal green fluorescence distribution at excitation and emission wavelengths of 488 and 520 nm, respectively. Of those cells exhibiting green fluorescence, only the brightest ∼73% were sorted and collected. This sorting threshold translated to approximately 20−40% of the entire cell population. The cells were maintained on an ice bath during the procedure.

Chemotaxis assays using a 48-well microchemotaxis (Boyden) chamber have been described elsewhere *(23)*. In brief, 10 μm pore size polycarbonate filters (PVP free; Neuro Probe Inc., MD) were soaked overnight in 0.1% w/v gelatin solution (Sigma Co.) to enhance cell adhesion to the substrate. Type IV collagen (CIV; Becton Dickinson Labware, MD) was dispersed into the media containing 0.1% fraction V bovine serum albumin (BSA; Sigma Co.) with 0.02 M HEPES in DMEM at a concentration of 100 μg/mL as the chemotactic solution. The pH of the chemotactic solution was adjusted to 7.4 prior to the experiment. The chemotactic solution was placed into the bottom wells of the 48-well chamber, and the cell suspension at 1.3×10^6 cells/mL was placed into the top wells, separated by a filter. The chamber assembly was placed into a 5% CO_2/37 °C environment for 4 h. The number of migrated cells was determined by staining filters using the DiffQuik staining kit (Dade International Inc., FL) and counting cells on the bottom side of the filter under 10× bright field magnification.

Micropipet Assay. The procedure for single micropipet assays was described in detail elsewhere *(24, 25)*. In brief, the cells were detached when subconfluent and allowed to regenerate for 1 h in culture medium. The cells were resuspended in serum-free DMEM containing 0.1% w/v BSA with 0.02 M HEPES, at 3.5×10^5 cells/mL. The cells were allowed to regenerate for an additional 1 h prior to the assay. A glass micropipet with 6.6 ± 0.4 μm i.d. was back-filled with chemotactic solution containing 100 μg/mL CIV with 0.1% BSA in serum-free DMEM plus 0.02 M HEPES. The loaded micropipet and a cell chamber containing sample A2058 cell suspension was placed

on the top of an inverted microscope stage. A freely suspended cell was held at the tip of the micropipet while applying a gentle aspiration pressure. The cell suspension and the experiment chamber contained 0.1% BSA in DMEM with 0.02 M HEPES. Cells were used in passages 14−20 for all experiments.

Micropipet Tethering Assay. Cells were detached when subconfluent and resuspended in media containing 0.1% w/v BSA and 0.02 M HEPES in DMEM at a concentration of 3.5×10^5 cell/mL. A 25 mm round glass coverslip was prepared by soaking overnight in 68 nM fibronectin (Becton Dickinson Labware) solution in order to enhance cell adhesion. The glass coverslip was mounted onto an experiment chamber, and the cell suspension was introduced into the prepared chamber 20 min prior to assay and mounted on the stage of an inverted microscope. A glass micropipet with 6.6 ± 0.4 μm i.d. was backfilled with the chemotactic solution containing 200 μg/mL CIV in DMEM with 0.1% w/v BSA and 0.02 M HEPES) and was held by a micromanipulator (Narishige Inc., Japan) and inserted into the experiment chamber atop the stage of a microscope. The tip of the glass micropipet containing CIV was placed approximately 10−15μm from the periphery of an adhered cell in the field of view. Fluorescence images under excitation/emission wavelengths of 488/520 nm were obtained every 15 min through a 35 mm camera (SC35; Olympus, Japan) mounted on a side port of the microscope.

Results

Expression of β-Actin−GFP. β-Actin−GFP was expressed as a fusion protein consisting of full-length β-actin with EGFP fused to the carboxy terminus. By use of fluorescence microscopy and flow cytometry, transient green fluorescence was detected and confirmed in NIH3T3, A2058, and 293T cells following transfection of β-actin−GFP expression construct. Approximately 30−50% of the cells were GFP positive following 18−24 h post-transfection. Fluorescence-activated cell sorting (FACS) was employed to select a population (30%) which maximally expressed β-actin−GFP (Figure 1A). The highest intensity of β-actin−GFP fluorescence was observed at approximately 24 h, and the intensity of β-actin−GFP fluorescence decayed with time until GFP expression was almost undetectable at 6 days post-transfection. Furthermore, FACS sorted β-actin−GFP cells failed to reach confluency, whereas EGFP controls did not exhibit loss of fluorescence or reduced confluency, possibly reflecting detrimental affects of overexpressing β-actin−GFP product.

Immuoblotting confirmed that β-actin−GFP fusion protein was being expressed. By use of an anti-β-actin antibody, 70 and 42 kD proteins were detected. The 70 kD band is consistent with the predicted molecular mass of β-actin−GFP fusion protein, whereas the 42 kD represents endogenous cellular β-actin (lane 4; Figure 1B). The total amount of β-actin−GFP fusion protein expressed was approximately 20% of the endogenous β-actin, as determined by densitometric measurements performed on the Western blot. Similar levels of expression of 42 kD endogenous β-actin were detected in all transfections indicating that the recombinant β-actin−GFP protein expression did not influence the expression of the endogenous β-actin in NIH3T3, A2058, and 293T cells. Furthermore, the identity of β-actin−GFP was confirmed using anti-GFP antibody for immunoblotting (Figure 1C). These observations indicate that although

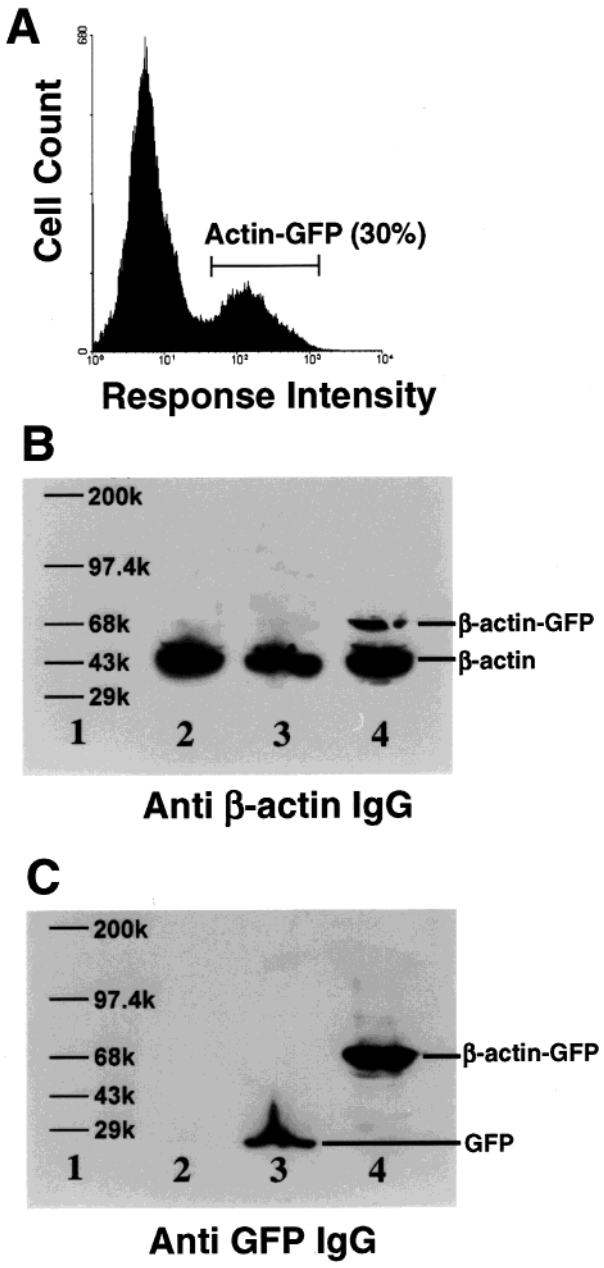

Figure 1. Ectopic expression of β-actin−GFP. (A) Histogram representing flow cytometry profiles of A2058 melanoma cells transfected with β-actin−GFP. Approximately 30% of the cells were positive for GFP. (B) Western blot for β-actin using whole-cell extracts from A2058 cells (lane 2), pEGFP transfected cells (lane 3), β-actin−GFP transfected cells (lane 4). Lane 1 represents MW standards. (C) Western blot of the above cell extracts for GFP.

overexpression of β-actin−GFP may be slightly detrimental, it can be expressed transiently in mammalian cells.

Intracellular Distribution of β-Actin−GFP Overlaps with Endogenous Actin Distribution. The above experiments indicate that β-actin−GFP can be expressed transiently in NIH3T3, A2058, and 293T cell lines; however, we were interested in determining whether this fusion protein could be employed for studying intracellular actin cytoskeleton distribution. Adherent cells growing on glass cover slips were fixed and stained with monomeric G-actin marker Texas Red conjugated DNase I to visualize the endogenous distribution of G-actin in untransfected, EGFP transfected, and β-actin−GFP transfected cells. In untransfected cells, the presence of Texas

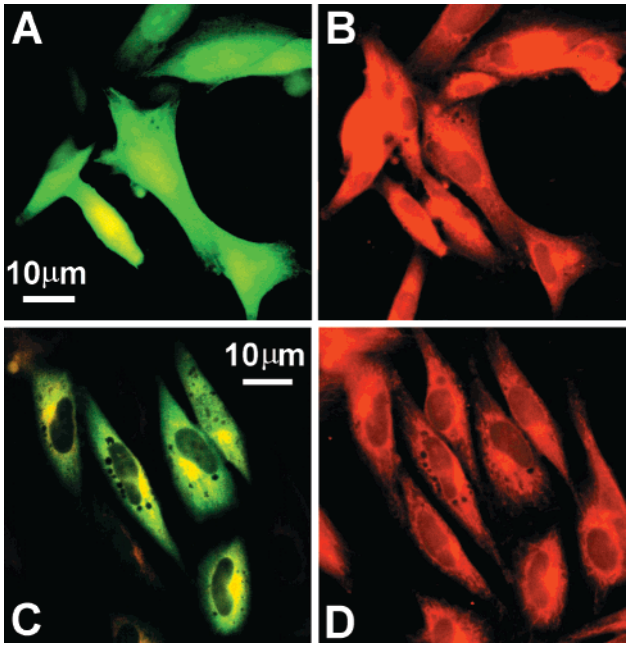

Figure 2. *β*-Actin−GFP colocalizes with A2058 cellular G-actin. (A) pEGFP transfected cells expressing GFP. (B) Monomeric actin in pEGFP transfected cells as determined by staining with Texas Red conjugated DNase I. (C) *β*-Actin−GFP transfected cells expressing fusion protein. (D) Monomeric actin distribution in *β*-actin−GFP cells as detected by DNase I staining. Images are at 40× magnification and are representative of eight experiments.

Red conjugated DNase I fluorescence was observed to be localized to cytoplasm, excluded from nucleus and concentrated at the perinuclear region as well as the cortical cell protrusions of A2058 cells. The A2058 cells transfected with pEGFP displayed a highly uniform green fluorescence throughout the cell cytosol including the nucleus (Figure 2A, B). More importantly, the nonspecific GFP distribution seemed to be discordant with monomeric G-actin as determined by DNase I staining. The *β*-actin−GFP fluorescence significantly overlapped the DNase I staining (Figure 2C, D). *β*-Actin−GFP was distributed similar to DNase I staining and was observed in the cytosol and concentrated in protrusions and the cortical region of cells while the nucleus remained unstained. This nonrandom fluorescent staining suggests that *β*-actin−GFP is participating in higher order actin cytoskeletal structures.

Furthermore, *β*-actin−GFP was shown to colocalize with stress fibers. 3T3 cells transfected with EGFP or *β*-actin−GFP were pretreated for 30 min in 15 *μ*M lysophosphatidic acid (LPA) to promote stress fiber formation. LPA has been shown to be a potent activator of small GTPase p21rho, an activator of stress fiber formation in vitro *(26−36)*. By use of Alexa Fluor 568 conjugated phalloidin, fixed NIH3T3 cells were stained, showing intracellular distribution of F-actin in the form of stress fibers. *β*-Actin−GFP transfected cells (Figure 3A) had green fluorescent stress fibers that closely matched phalloidin stained fibers in LPA-treated controls (Figure 3B). Negative controls included EGFP transfectants which expressed GFP throughout the cytosol and nucleus despite the induction of stress fiber formation (Figure 3C). Taken together, these experiments demonstrate that the distribution of *β*-actin−GFP can be found within the cell as monomeric G- or polymerized F-actin and can be used as an accurate indication of intracellular actin structure.

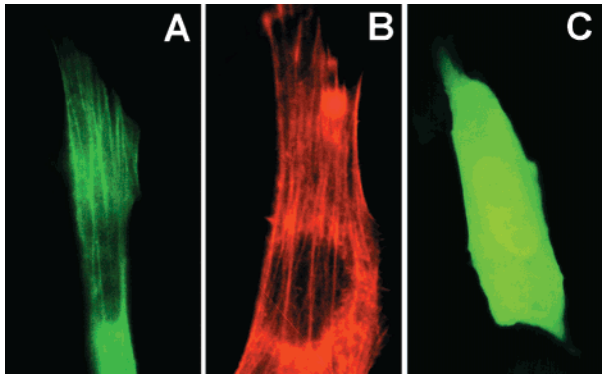

Figure 3. *β*-Actin−GFP colocalizes with NIH3T3 cellular F-actin. (A) *β*-Actin−GFP transfected cells expressing fusion protein. (B) Polymerized F-actin in cells as determined by staining with Alexa Fluor 568 conjugated phalloidin. (C) pEGFP transfected cells expressing GFP. Images A and C are at 100× magnification, and image B is at 150× magnification. All images are representative of eight experiments.

Redistribution of *β*-Actin−GFP During Cell Migration and Pseudopodial Protrusion. Chemotaxis requires reorganization of the cytoskeleton including *β*-actin polymers *(1−3, 5, 6)*. To determine if the *β*-actin−GFP fusion protein could be used for studying actin reorganization during chemotaxis, we used the melanoma cell line A2058. A2058 cells have been shown to respond to CIV as a chemotactic solution *(37, 38)*, and we used this chemoattractant and a Boyden chamber to determine the motility of A2058 cells that were overexpressing *β*-actin−GFP. Nontransfected control cells migrated 3475 ± 690 cells per well (3.17 mm^2), whereas *β*-actin−GFP transfectants migrated 3001 ± 573 cells per well (Figure 4). These results indicate that the chemotactic properties of A2058-*β*-actin−GFP and nontransfected controls are comparable and that the former cells can be used as a model system for cell motility assays.

The ability of *β*-actin−GFP to be incorporated into higher order actin networks was further investigated by using a previously described assay for monitoring pseudopodia formation in response to a chemoattractant *(24, 25)*. This assay uses a glass micropipet for local delivery of CIV to a target cell. Responsive cells extend pseudopodia into the micropipet which harbors a high concentration of CIV. Figure 5 shows that CIV effectively stimulates A2058 and A2058-*β*-actin−GFP cells in a similar fashion. Pseudopodial protrusion began within the first 15 min of cell-to-pipet focal contact and irregularly extended into the micropipet for the duration of the assay (Figure 5A−D). The time course of pseudopodial formation, the pseudopodial length, and structure did not appear to be compromised and were similar to previous results *(24)*. EGFP transfected cells exhibited uniformly green fluorescence within the cell body and in the protruding pseudopod (Figure 5M−P). This diffuse GFP distribution hindered observations of higher order intracellular structures. In contrast to the EGFP, *β*-actin−GFP fluorescence was shown to be distributed nonuniformly within the pseudopods and in the cell body (Figure 5E−H). To visualize the distribution of actin in a suspended viable cell, sequential images were taken at 15 min intervals. Initially, a diffuse *β*-actin−GFP fluorescence was observed when the cell was held at the tip of the micropipet. When a protrusion was initiated by chemoattractant, an increase in *β*-actin−GFP was qualitatively observed in the extended process and the entire thin cortical regions adjacent to the cell surface. With time, the fluorescence became more distinct in these

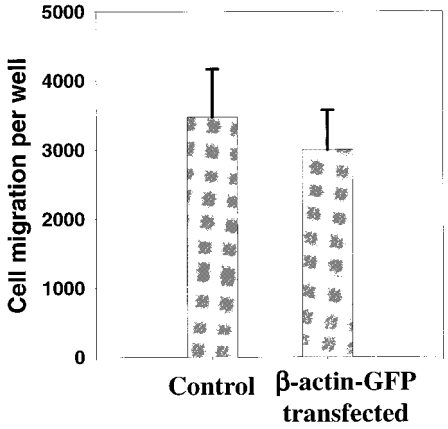

Figure 4. Motility of β-actin−GFP overexpressing cells. Cell motility of untransfected control and β-actin−GFP transfected cells in response to 100 μg/mL CIV was assayed in chemotaxis wells as described in Materials and Methods. The results represent six independent experiments of 36 chemotaxis wells, shown with ±SD. Untransfected control cells migrated 3475 ± 690 while β-actin−GFP transfectants migrated 3001 ± 573 per well (3.17 mm^2) at $p < 0.001$ (Student t-test, assuming unequal variance). Background baseline motility (9% ± 1% of control) was subtracted from the presented results.

cells; this was consistent with the continuous recruitment of β-actin−GFP to the pseudopodia. Relative distribution of the green fluorescence continually changed over the time course of an experiment. We were able to monitor changes in actin organization for approximately 1 h before the signal was substantially diminished by photobleaching from repeated UV exposure. For comparison, we fixed cells at various times following CIV treatment and stained them with fluorescent phalloidin. The pattern of phalloidin staining was very similar to what was observed with β-actin−GFP, both within the pseudopodia and in the cell body (Figure 5I−L). These data support the conclusion that β-actin−GFP exhibit a qualitative reorganization that reflects F-actin remodeling induced by chemotaxis in a viable cell.

Actin Dynamics Observed in Micropipet Tethering Assay. The above experiments permit the real-time examination of actin dynamics during pseudopodial protrusion and chemotaxis. Similar reorganization of the actin network would be expected in cells crawling toward a chemoattractant, and it may be possible to visualize these events with β-actin−GFP. Cells were placed in a chemoattractant gradient, and the ability of cells to crawl was monitored. Furthermore, images obtained sequentially allowed an observation of the real-time cell crawling response following the direction of chemoattractant concentration gradient. Representative images were acquired every 15 min, beginning with the initial placement of the micropipet as the starting point of an assay (Figure 6). We first attempted to observe those cells expressing EGFP crawling toward the source of CIV chemoattractant. EGFP transfected cells exhibited green fluorescence uniformly throughout the cell cytoplasm (Figure 6A−E). In these cells, both the leading edge protrusions and the cell cytosol contained evenly distributed green fluorescence, indicating that EGFP cellular localization cannot be used as an indicator of cytoskeleton reorganization. In contrast to EGFP transfected cells, β-actin−GFP had a distinct pattern of intracellular staining during the assay (Figure 6F−J). Small protrusions and projections with relatively high intensities of green fluorescence were observed along the periphery of the cell at the beginning of an experiment. During the course of the assay, the polarized cell was shown to extend protrusions containing high intensities of green fluorescence in the direction of the micropipet tip. The lagging end did not increase green fluorescence intensity during the assay, whereas the extending pseudopodial projections were brightly fluorescent at the focal tip, indicating a high concentration of β-actin−GFP. These data indicate that a distinct cell polarity was induced by CIV stimulation and suggest that β-actin−GFP can be used to examine real-time changes in the cytoskeleton in a viable cell system.

Discussion

In this study, β-actin−GFP was demonstrated to be an efficient and effective tool for monitoring the dynamic actin distribution within a viable cell. The observed distribution of β-actin−GFP fluorescence was consistent with those seen using fixed-cell immunofluorescence staining methods *(7−10, 39−42)*, indicating that β-actin−GFP was incorporated into the cytoskeleton immediately after its expression. Although other studies in *Dictyostelium*, yeast, and some mammalian cells *(12, 18, 20)* have suggested that *Dictyostelium* actin-15 conjugated GFP was capable of copolymerizing with the endogenous cellular actin, we utilized human β-actin cDNA to eliminate any possibility of cross-species affects. Previously, Choidas et al. used *Dictyostelium*-actin−GFP to characterize actin organization in several cell types including rat bladder cells induced to undergo transformation *(12)*. Furthermore, Robbins et al. utilized GFP conjugated human β-actin to examine the formation of membrane protrusions following *L. monocytogenes* infection of MDCK cells *(13)*. While these previous studies demonstrated the utility of GFP conjugated actin in more traditional cell motility assay systems, we have extended the application of β-actin−GFP with our in vitro micropipet pseudopodial protrusion and tumor cell migration assay systems. Using β-actin−GFP in these systems, we measured and documented biophysical and kinetic parameters including rate and frequency of pseudopodial protrusion and chemotactic cell migration to specific chemoattractant *(2, 24, 25, 38)*.

We have shown by immunostaining that β-actin−GFP fluorescence significantly overlapped with the endogenous G- and F-actin distributions. Furthermore, β-actin−GFP transfectants exhibited normal pseudopodial protrusions during a micropipet assay, and cell tethering experiments revealed a distinct recruitment of β-actin−GFP to the leading edge of protrusions during chemotaxis. These results indicated that β-actin−GFP preserved the basic function of actin, with minimal side effects.

Since actin rearrangement and contraction of the cell cortex are believed to be involved in the extension of pseudopodial protrusions *(5, 43, 44)*, the current study indicates that the β-actin−GFP does not significantly interfere with normal cellular actin reorganization in response to a chemotactic signal. However, the β-actin−GFP transfected cells exhibited reduced growth, suggesting that GFP conjugated actin reduced cytokinesis in culture. Although there are reports of stable cell lines that overexpress actin−GFP in the literature *(12−14)*, others have observed similar detrimental affects following ectopic actin−GFP expression *(19, 45)*. Aizawa et al. have suggested a reduction in the rate and efficiency of polymerization of actin−GFP as a possible cause for this phenotype in *Dictyostelium (19)*. Magdolen et al. have observed that ectopic actin expression in yeast was lethal, whereas sequestration of actin monomers by an overproduction of profilin suppressed this phenotype *(45)*. The

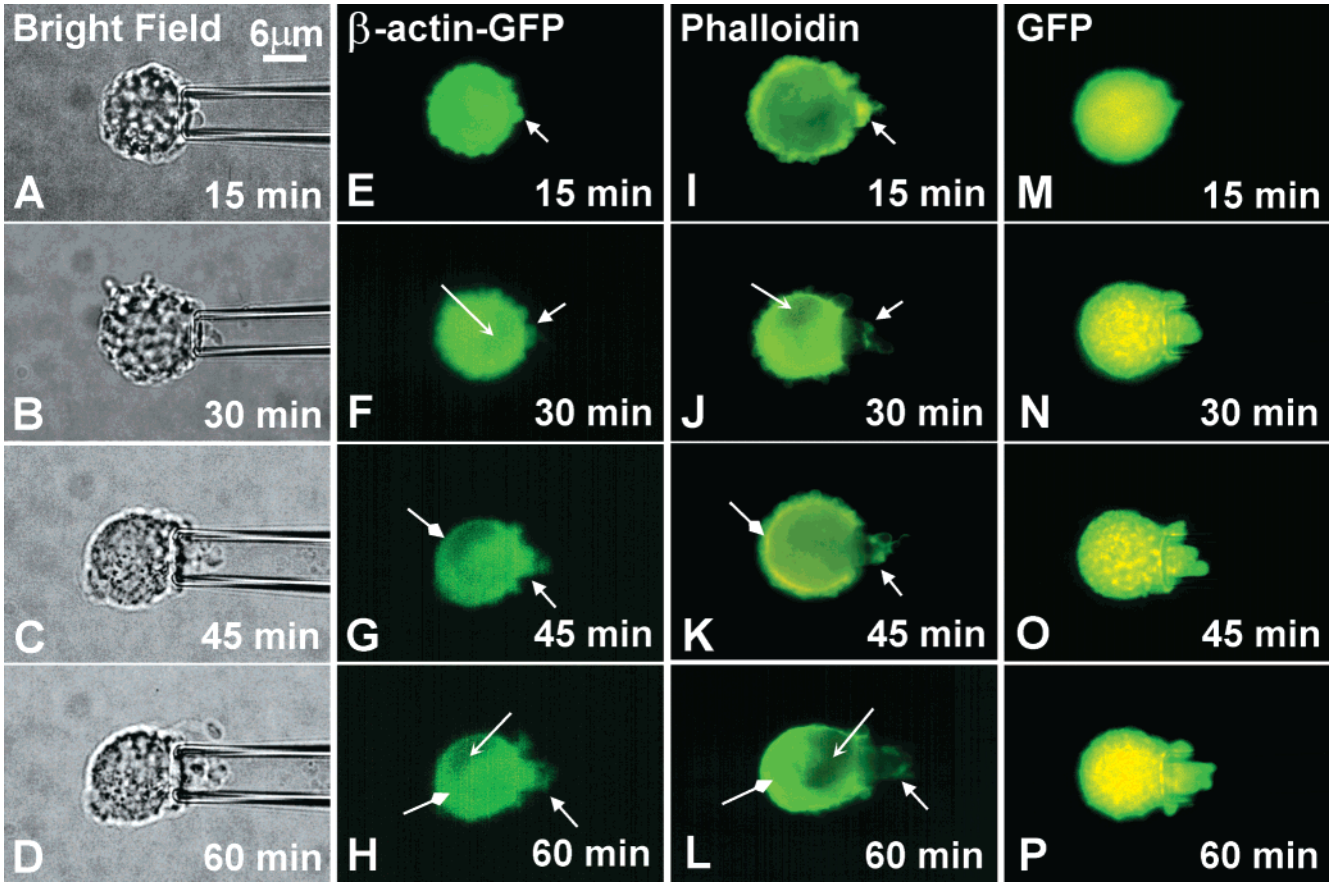

Figure 5. β-Actin−GFP localizes to protruding pseudopods in response to chemoattractants. Panels show representative images of a suspended A2058 melanoma cell protruding pseudopods in response to 100 μg/mL type IV collagen stimulation within the glass micropipet. Panels (A)−(D) show bright field images at 100× magnification. Panels (E)−(H) show the β-actin−GFP distribution in the same cell. Panels (I)−(L) show the F-actin distribution in representative cells using Alexa Fluor 488 conjugated phalloidin. Panels (M)−(P) show the GFP distribution in a pEGFP transfected cell. Images were acquired every 15 min from the initial cell to pipet contact. Various arrows indicate locations of similarity between β-actin−GFP transfectants and phalloidin stained cells. Results are representative of 8−10 independent experiments.

apparent cytotoxicity of β-actin−GFP that we observed is limited to long-term cultures. We saw little differences in the chemotactic properties of β-actin−GFP expressing cells and controls, suggesting that for motility and metastasis assays, the time frame is too short to negatively impact our results. More importantly, our observations indicate that β-actin−GFP is a useful reagent for studying cytoskeleton changes during chemotaxis.

We have previously established an in vitro system to study pseudopod formation wherein suspended tumor cells are stimulated to form pseudopods into drawn glass pipets containing CIV *(24, 25)*. Using β-actin−GFP transformed cells, we were able to follow the dynamic distribution and polarization of the actin network in a whole cell as well as within the focal pseudopodial and lamellipodial formations. Although the relationship between CIV-induced signal transduction and cortical actin reorganization is presently unclear, there are data indicating that some chemoattractants induce cell polarization via focal accumulation of F-actin *(36)*. It is also likely that cell adhesion and the extent of chemotactic receptor engagement may affect whole-cell polarization and actin rearrangement in highly motile tumor cells *(46−52)*. Since local actin polymerization is an initial cellular event leading to cell polarization and protrusion of pseudopods, filopods, and lamellipods *(5, 44)*, we have successfully used β-actin−GFP to observe the dynamic real-time recruitment of actin within the tips of these extending cellular processes.

We were able to observe significant changes in the actin structure within the cortical cytoskeleton during chemotaxis. Changes in F-actin organization, or more precisely, the cross-linking of actin filaments by actin-binding proteins occupying a region adjacent to the cell surface have been proposed to provide the structural integrity to the pseudopods *(1, 5, 6, 44)*. Changes observed in the A2058 cell cortex in response to a gradient of CIV from a micropipet not only involved local regions, but most of the cortical structure within the cell as revealed by our β-actin−GFP protein and phalloidin fluorescence stain. During the early stages, the shape of the suspended A2058 cell remained spherical and a thin cortical submembranous layer was observed along the entire cell surface. However, at approximately 30 min post-CIV exposure, an accumulation of β-actin−GFP was observed within the protruding pseudopodia as well as near the membrane at the opposite side of the protrusion. This was followed by a gradual contraction of the cell body which in turn lead to a further advancement of the pseudopodia into the lumen of the glass pipet. The contractile force of this region of the cortex may have generated an internal pressure difference between the cell body and the stimulated region, thereby creating a mass flux into extending pseudopods, further reinforcing the cell polarity.

We have shown that recombinant β-actin−GFP transformed cells can be used efficiently and effectively to monitor the real-time dynamics of actin cytoskeleton

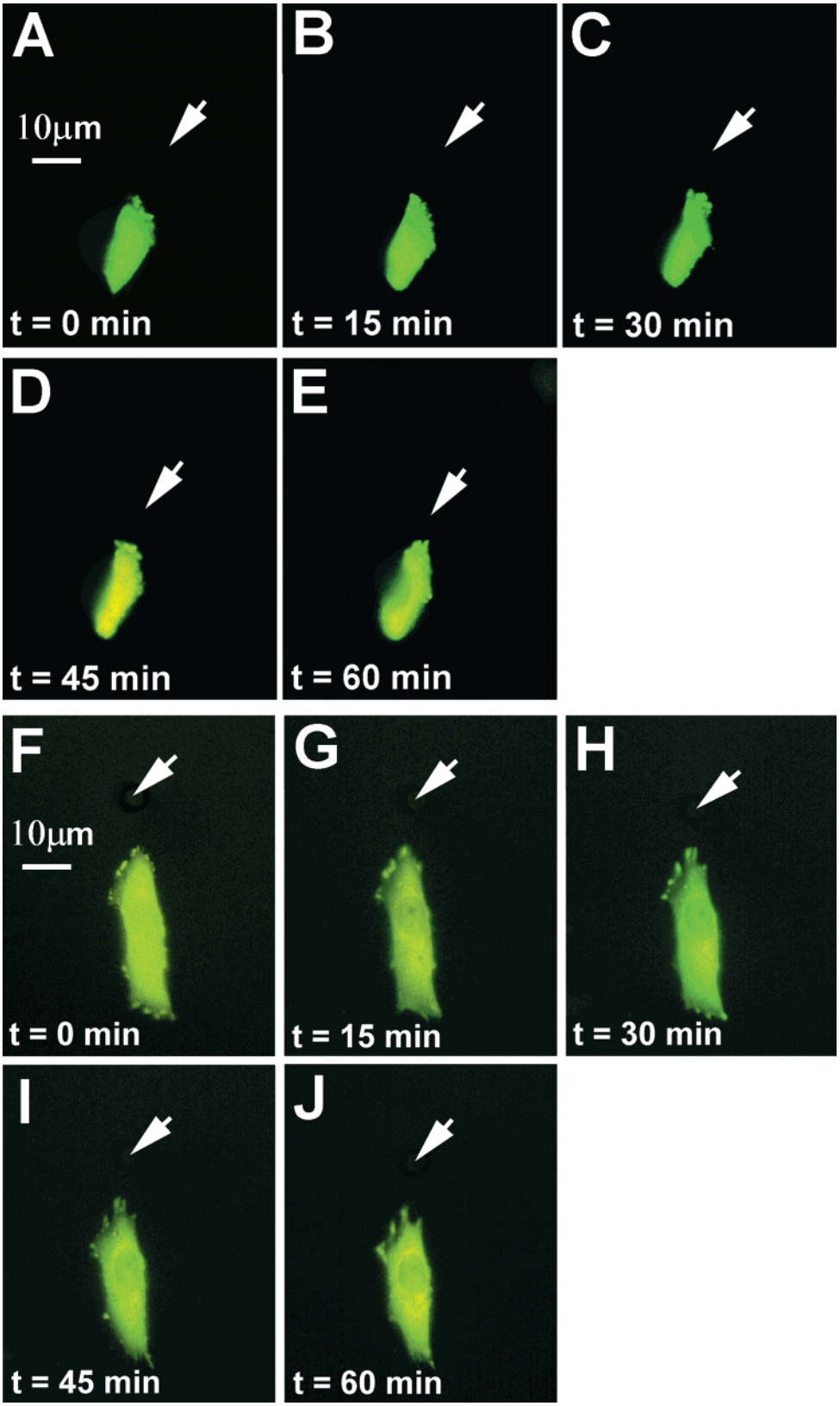

Figure 6. β-Actin−GFP localizes to the leading edge in response to chemoattractant. Representative images of an adhered A2058 melanoma cell tethered-chemotaxis toward a glass micropipet containing 200 μg/mL type IV collagen are shown. The tip of the micropipet is shown with a white arrow. In panels (A)−(E), EGFP transfected cell response is shown, whereas panels (F)−(J) show β-actin−GFP transfected cell. All images are at 40× magnification.

rearrangements in response to extracellular chemotactic stimuli in vitro. By transfecting a β-actin−GFP expression construct into cells, we were able to avoid potential side effects that are usually associated with more invasive methods such as microinjection and cell fixation. Furthermore, we used this fusion protein to examine the mechanism of cellular signaling and pseudopodial extension during CIV chemotaxis. These studies demonstrate that β-actin−GFP is an effective tool for visualizing actin rearrangements in a viable cell system.

Conclusion

An expression vector encoding a fusion protein consisting of *Aequorea victoria* green fluorescent protein (GFP) and human β-actin was transfected into NIH3T3 fibroblast, A2058 human melanoma, and 293T human embryonic kidney carcinoma cell lines. The expressed β-actin−GFP fusion protein colocalized with endogenous cellular actin as determined by histoimmunofluorescence staining. By use of this β-actin−GFP, dynamics of cytoskeletal actin were observed in real-time during an active cell chemotaxis toward extracellular matrix protein type IV collagen as the chemoattractant. Cellular pseudopodial protrusions and cortical structures of collagen stimulated cells exhibited distinct and continually changing recruitment patterns of β-actin−GFP during chemotaxis. We report the first in vitro observations of actin dynamics in a viable cell during an active chemotactic response toward type IV collagen. The novel application of β-actin−GFP to cell motility studies enabled noninvasive means of characterizing the intracellular cytoskeleton dynamics.

Acknowledgment

Authors acknowledge the support for this research from NSF-BES-9502069 (C.D. is a recipient of NSF Faculty Career Award) and NIH-CA-76434 (C.D.). The technical assistance of Linh Truong, Huiyu Zhou, Deba Sarma, and Eileen Lee are also acknowledged. We thank Elaine Kunze at Penn State Cell Sorting facility for assistance in quantitative FACS analysis and William O. Hancock, Norman R. Harris, and Herbert H. Lipowsky at Penn State University Bioengineering Department for valuable discussions.

References and Notes

(1) Alberts, B.; Bray, D.; Lewis, J.; Raff, M.; Roberts, K.; Watson, J. D. In *Molecular Biology of The Cell*; Garland Publishing Inc.: New York, 1994; pp 721−858; 950−1006; 1255−1269.

(2) Aznavoorian, S. A.; Stracke, M. L.; Krutzsch, H.; Schiffmann, E.; Liotta, L. A. Signal Transduction for Chemotaxis and Haptotaxis by Matrix Molecules in Tumor Cells. *J. Cell Biol.* **1990**, *110*, 1427−1438.

(3) Lester, B. R.; McCarthy, J. B. Tumor Cell Adhesion to the Extracellular Matrix and Signal Transduction Mechanism Implicated in Tumor Cell Motility, Invasion and Metastasis. *Cancer Metastasis Rev.* **1992**, *11*, 31−44.

(4) Schnaper, H. W.; Kleinman, H. K. Regulation of Cell Function by Extracellular Matrix. *Pediatr. Nephrol.* **1993**, *7*, 96−104.

(5) Stossel, T. P. On the Crawling of Animal Cells. *Science* **1993**, *260*, 1086−1094.

(6) Bray, D. In *Cell Movements*; Garland Publishing: New York, 1992; pp 143−153; 341−354.

(7) Wang, Y. L. Exchange of Actin Subunits at the Leading Edge of Living Fibroblasts: Possible Role of Treadmilling. *J. Cell Biol.* **1985**, *101*, 597−602.

(8) Theriot, J. A.; Mitchison, T. J. Actin Microfilament Dynamics in Locomoting Cells. *Nature* **1991**, *352*, 126−131.

(9) Zhelev, D. V.; Hochmuth, R. M. Mechanically Stimulated Cytoskeleton Rearrangement and Cortical Contraction in Human Neutrophils. *Biophys. J.* **1995**, *68*, 2004−2014.

(10) Taylor, D. L.; Wang, Y. L. Molecular Cytochemistry: Incorporation of Fluorescently Labeled Actin into Living Cells. *Proc. Natl. Acad. Sci. U.S.A.* **1978**, *75*, 857−861.

(11) Farina, K. L.; Wyckoff, J. B.; Rivera, J.; Lee, H.; Segall, J. E.; Condeelis, J. S.; Jones, J. G. Cell Motility of Tumor Cells Visualized in Living Intact Primary Tumors Using Green Fluorescent Protein. *Cancer Res.* **1998**, *58*, 2528−2532.

(12) Choidas, A.; Jungbluth, A.; Sechi, A.; Murphy, J.; Ullrich, A.; Marriott, G. The Suitability and Application of a GFP−Actin Fusion Protein for Long-Term Imaging of the Organization and Dynamics of the Cytoskeleton in Mammalian Cells. *Eur. J. Cell Biol.* **1998**, *77*, 81−90.

(13) Robbins, J. R.; Barth, A. I.; Marquis, H.; de Hostos, E. L.; Nelson, W. J.; Theriot, J. A. *Listeria Monocytogenes* Exploits Normal Host Cell Processes to Spread from Cell to Cell. *J. Cell Biol.* **1999**, *146*, 1333−1349.

(14) Fischer, M.; Kaech, S.; Knutti, D.; Matus, A. Rapid Actin-Based Plasticity in Dendritic Spines. *Neuron* **1998**, *20*, 847−854.

(15) Misteli, T.; Spector, D. L. Application of the Green Fluorescent Protein in Cell Biology and Biotechnology. *Nat. Biotechnol.* **1997**, *15*, 961−964.

(16) Sheen, J.; Hwang, S.; Niwa, Y.; Kobayashi, H.; Galbraith, D. W. Green-Fluorescent Protein as a New Vital Marker in Plant Cells. *Plant J.* **1995**, *8*, 777−784.

(17) Edwards, K. A.; Demsky, M.; Montague, R. A.; Weymouth, N.; Kiehart, D. P. GFP−Moesin Illuminates Actin Cytoskeleton Dynamics in Living Tissue and Demonstrates Cell Shape Changes during Morphogenesis in *Drosophila*. *Dev. Biol.* **1997**, *191*, 103−117.

(18) Westphal, M.; Jungbluth, A.; Heidecker, M.; Mòhlbauer, B.; Heizer, C.; Schwartz, J. M.; Marriott, G.; Gerisch, G. Microfilament Dynamics During Cell Movement and Chemotaxis Monitored Using GFP-Actin Fusion Protein. *Curr. Biol.* **1997**, *7*, 176−183.

(19) Aizawa, H.; Sameshima, M.; Yahara, I. A Green Fluorescent Protein-Actin Fusion Protein Dominantly Inhibits Cytokinesis, Cell Spreading, and Locomotion in *Dictyostelium*. *Cell Struct. Funct.* **1997**, *22*, 335−345.

(20) Doyle, T.; Botstein, D. Movement of Yeast Cortical Actin Cytoskeleton Visualized in Vivo. *Proc. Natl. Acad. Sci. U.S.A.* **1996**, *93*, 3886−3891.

(21) Verkhusha, V. V.; Tsukita, S.; Oda, H. Actin Dynamics in Lamellipodia of Migrating Border Cells in the *Drosophila* Ovary Revealed by GFP-Actin Fusion Protein. *FEBS Lett.* **1999**, *445*, 395−401.

(22) Maniatis, T.; Sambrook, J.; Fritsch, E. F. In *Molecular Cloning: A Laboratory Manual*; Cold Spring Harbor Laboratory: New York, 1989.

(23) Harvath, L.; Falk, W.; Leonard, E. J. Rapid Quantitation of Neutrophil Chemotaxis: Use of a Poly(vinylpyrrolidone)-free Polycarbonate Membrane in a Multiwell Assembly. *J. Immunol. Methods* **1980**, *37*, 39−45.

(24) Dong, C.; Aznavoorian, S. A.; Liotta, L. A. Two Phases of Pseudopod Protrusion in Tumor Cells Revealed by a Micropipet. *Microvasc. Res.* **1994**, *47*, 55−67.

(25) Dong, C.; You, J.; Aznavoorian, S. A.; Savarese, D. M. F.; Liotta, L. A. In *Cell Mechanics and Cellular Engineering*; Mow, V. C., Ed.; Springer-Verlag: New York, 1994; pp 515−533.

(26) Krannenburg, O.; Poland, M.; Gebbink, M.; Oomen, L.; Moolenaar, W. H. Dissociation of LPA-Induced Cytoskeletal Contraction from Stress Fiber Formation by Differential Localization of Rho A. *J. Cell Sci.* **1997**, *110*, 2417−2427.

(27) Moolenaar, W. H. Lysophosphatidic Acid, A Multifunctional Phospholipid Messenger. *J. Biol. Chem.* **1995**, *270*, 12949−12952.

(28) Seufferlein, T.; Rozengurt, E. Lysophosphatidic Acid Stimulates Tyrosine Phosphorylation of Focal Adhesion Kinase, Paxillin, and p130. *J. Biol. Chem.* **1994**, *269*, 9345−9351.

(29) Schaller, M. D.; Parsons, J. T. Focal Adhesion Kinase and Associated Proteins. *Curr. Opin. Cell Biol.* **1994**, *6*, 705−710.

(30) Barry, S. T.; Critchley, D. R. The Rho A-Dependent Assembly of Focal Adhesions in Swiss 3T3 Cells is Associated with Increased Tyrosine Phosphorylation and the Recruitment of both pp125FAK and Protein Kinase C-δ to Focal Adhesions. *J. Cell Sci.* **1994**, *107*, 2033−2045.

(31) Ridley, A. J. Rho-Related Proteins: Actin Cytoskeleton and Cell Cycle. *Curr. Opin. Genet. Dev.* **1995**, *5*, 24−30.

(32) Ridley, A. J.; Hall, A. Signal Transduction Pathways Regulating Rho-Mediated Stress Fiber Formation: Requirement for a Tyrosine Kinase. *EMBO J.* **1994**, *13*, 2600−2610.

(33) Zigmond, S. H. Signal Transduction and Actin Filament Organization. *Curr. Opin. Cell Biol.* **1996**, *8*, 66−73.

(34) Tapon, N.; Hall, A. Rho, Rac and Cdc42 GTPases Regulate the Organization of the Actin Cytoskeleton. *Curr. Opin. Cell. Biol.* **1997**, *9*, 86−92.
(35) Hall, A. Small GTP−Binding Proteins and the Regulation of the Actin Cytoskeleton. *Annu. Rev. Cell Biol.* **1994**, *10*, 31−54.
(36) Macheskey, L. M.; Hall, A. Role of Actin Polymerization and Adhesion to Extracellular Matrix in Rac- and Rho-Induced Cytoskeletal Reorganization. *J. Cell Biol.* **1997**, *138*, 913−926.
(37) Savarese, D. M. F.; Russell, J. T.; Fatatis, A.; Liotta, L. A. Type IV Collagen Stimulates an Increase in Intracellular Calcium. *J. Biol. Chem.* **1992**, *267*, 21928−21935.
(38) Stracke, M. L.; Aznavoorian, S. A.; Beckner, M. E.; Liotta, L. A.; Schiffmann, E. Cell Motility, A Principal Requirement for Metastasis. In *Cell Motility Factors*; Birkhauser Verlag: Bassel, Switzerland, 1991; pp 148−161.
(39) DuBose, D. A.; Haugland, R. P. Comparisons of Endothelial Cell G- and F−Actin Distribution in Situ and in Vitro. *Biotech. Histochem.* **1993**, *68*, 8−16.
(40) Sanger, J. M.; Dabiri, G.; Mittal, B.; Kowalski, M. A.; Haddad, J. G.; Sanger, J. G. Disruption of Microfilament Organization in Living Nonmuscle Cells by Microinjection of Plasma Vitamin D-Binding Protein or DNase I. *Proc. Natl. Acad. Sci. U.S.A.* **1990**, *87*, 5474−5478.
(41) Haugland, R. P.; You, W.; Paragas, V. B.; Wells, K. S.; DuBose, D. A. Simultaneous Visualization of G- and F-Actin in Endothelial Cells. *J. Histochem. Cytochem.* **1994**, *42*, 345−350.
(42) Knowles, G. C.; McCulloch, A. G. Simultaneous Localization and Quantification of Relative G- and F-Actin Content: Optimization of Fluorescence Labeling Methods. *J. Histochem. Cytochem.* **1992**, *40*, 1605−1612.
(43) Condeelis, J. S. In *Motion Analysis of Living Cells*; Wiley-Liss, Inc.: New York, 1998; pp 85−100.
(44) Mogilner, A.; Oster, G. Cell Motility Driven by Actin Polymerization. *Biophys. J.* **1996**, *71*, 3030−3045.
(45) Magdolen, V.; Drubin, D. G.; Mages, G.; Bandlow, W. High Levels of Profilin Suppress the Lethality Caused by Overproduction of Actin in Yeast Cells. *FEBS Lett.* **1993**, *316*, 41−47.
(46) Schwartz, M. A.; Schaller, M. D.; Ginsberg, M. H. Integrins: Emerging Paradigms of Signal Transduction. *Annu. Rev. Cell Dev. Biol.* **1995**, *11*, 549−599.
(47) Schwartz, M. A.; Toksoz, D.; Khosravi-Far, R. Transformation by Rho Exchange Factor Oncogenes is Mediated by Activation of an Integrin-Dependent Pathway. *EMBO J.* **1996**, *15*, 6525−6530.
(48) Fernandez, R.; Boxer, L. A.; Suchard, S. J. Beta 2 Integrins are Not Required for Tyrosine Phosphorylation of Paxillin in Human Neutrophils. *J. Immunol.* **1997**, *159*, 5568−5575.
(49) Masur, S. K.; Idris, A.; Mechelson, K.; Antohi, S.; Zhu, L. X.; Weissberg, J. Integrin-Dependent Tyrosine Phosphorylation in Corneal Fibroblasts. *Invest. Ophthalmol. Vis. Sci.* **1995**, *36*, 1837−1846.
(50) Tawil, N.; Wilson, P.; Carbonetto, S. Integrin in Point Contacts Mediate Cell Spreading: Factors that Regulate Integrin Accumulation in Point Contacts vs. Focal Contacts. *J. Cell Biol.* **1993**, *120*, 261−271.
(51) Eddy, R. J.; Han, J.; Condeelis, J. S. Capping Protein Terminates but Does Not Initiate Chemoattractant-Induced Actin Assembly in *Dictyostelium*. *J. Cell Biol.* **1997**, *139*, 1243−1253.
(52) Chan, A. Y.; Raft, S.; Bailly, M.; Wyckoff, J. B.; Segall, J. E.; Condeelis, J. S. EGF Stimulates an Increase in Actin Nucleation and Filament Number at the Leading Edge of the Lamellipod in Mammary Adenocarcinoma Cells. *J. Cell Sci.* **1998**, *111*, 199−211.

Accepted for publication July 31, 2000.

BP000093O